


Article

Visible Light Enhanced Extracellular Electron Transfer between a Hematite Photoanode and *Pseudomonas aeruginosa*

Guiping Ren ^{1,2} , Yuan Sun ^{1,2}, Manyi Sun ^{1,2}, Yan Li ^{1,2}, Anhuai Lu ^{1,2,*} and Hongrui Ding ^{1,2,*}

¹ The Key Laboratory of Orogenic Belts and Crustal Evolution, School of Earth and Space Sciences, Peking University, Beijing 100871, China; renguiping@pku.edu.cn (G.R.); sess_sy@pku.edu.cn (Y.S.); 1601210285@pku.edu.cn (M.S.); liyan-pku@pku.edu.cn (Y.L.)

² Beijing Key Laboratory of Mineral Environmental Function, Peking University, Beijing 100871, China

* Correspondence: ahlu@pku.edu.cn (A.L.); DHR@pku.edu.cn (H.D.); Tel.: +86-10-6275-3555 (A.L.)

Received: 23 October 2017; Accepted: 20 November 2017; Published: 23 November 2017

Abstract: Exploring the interplay between sunlight, semiconducting minerals, and microorganisms in nature has attracted great attention in recent years. Here we report for the first time the investigation of the interaction between a hematite photoelectrode and *Pseudomonas aeruginosa* PAO1 under visible light irradiation. Hematite is the most abundant mineral on earth, with a band gap of 2.0 eV. A hematite electrode was electrochemically deposited on fluorine-doped tin oxide (FTO). It was thoroughly characterized by environmental scanning electron microscopy (ESEM), Raman, and UV–Vis spectroscopy, and its prompt response to visible light was determined by linear sweep voltammetry (LSV). Notably, under light illumination, the hematite electrode immersed in a live cell culture was able to produce 240% more photocurrent density than that in the abiotic control of the medium, suggesting a photoenhanced extracellular electron transfer process occurring between hematite and PAO1. Different temperatures of LSV measurements showed bioelectrochemical activity in the system. Furthermore, I–t curves under various conditions demonstrated that both a direct and an indirect electron transferring process occurred between the hematite photoanode and PAO1. Moreover, the indirect electron transferring route was more dominant, which may be mainly attributed to the pyocyanin biosynthesized by PAO1. Our results have expanded our understanding in that in addition to *Geobacter* and *Shewanella* it has been shown that more microorganisms are able to perform enhanced extracellular electron transfer with semiconducting minerals under sunlight in nature.

Keywords: hematite; photoanode; *Pseudomonas aeruginosa* PAO1; extracellular electron transfer

1. Introduction

The global cycling of organic matter and elements is driven to a great extent by microorganisms with the ability to exchange electrons with extracellular substrates, such as oxidized or reduced soluble and insoluble metals and other microorganisms [1–3]. Over the past few decades, exploiting the capability of extracellular electron transfer (EET) for microorganisms has attracted great attention in the field of environmental microbiology, geomicrobiology, and even environmental remediation applications [4–6]. Redox-active minerals, such as those that contain iron and manganese oxide minerals, are abundant in soils and in aquatic and subsurface sediments, which electrically support microbial growth in different kinds of ways [7]. Among a wide variety of Fe oxide minerals, hematite is the most widespread type on earth which has been demonstrated to work as the most common natural electron acceptor for the EET process by dissimilatory metal-reducing microorganisms [8–11]. However, one significant question has been overlooked in that hematite and some Fe/Mn oxides are

semiconductive [12]. Under light, these oxides are likely to interact differently with microorganisms during the electron exchange processes and may also have an impact on the microbial EET activities via structural rearrangements or surface chemical reactions [3,13].

Recently, some progress has been made in the investigation of electron transfer between semiconducting minerals and microorganisms under solar illumination, the solar-assisted microbial photoelectrochemical system has been developed as well [14–19]. Li et al. reported that most bioelectrons from *Geobacter sulfurreducens* were transferred to the conduction band of hematite and further delivered to the ITO (Indium Tin Oxides) electrode and the light-induced electron transfer correlated linearly with the rates of microbial respiration [16]. Qian et al. observed the enhanced photocurrent of the solar-assisted microbial photoelectrochemical system, suggesting a photo-enhanced electrochemical interaction between hematite and *Shewanella oneidensis* MR-1 [17]. Furthermore, the performance of bio-engineered *Shewanella oneidensis* MR-1 with hematite nanowire-arrayed photoanode was investigated, enhanced photocurrents being produced as well [18]. In addition, the bacterial community in photo-bioelectrochemical systems was analyzed and the author suggested that the main role of the photobioanode was to accelerate biofilm formation, enrich exoelectrogens, and enhance extracellular electron transfer [19]. Up to now, there have been relatively few studies devoted to the interactions of the light-semiconducting minerals–microorganism system, and the numbered researches mainly focus on the model bacteria of *Geobacter* and *Shewanella*, unfortunately other microorganism have been overlooked. The mechanisms controlling the extracellular electron transfer between bacteria and semiconducting minerals under solar irradiation have not been adequately identified until now. Further efforts are required to understand the EET process between microorganisms and mineral photocatalysis under solar illumination.

Pseudomonas aeruginosa is a Gram-negative, rod-shaped bacterium of ubiquitous occurrence in the environment [20]. This species contains lots of different strains and which are dominant in microbial fuel cells (MFC). Moreover, most of the strains can use nitrate/nitrite or oxygen as electron acceptors [21,22]. The electrochemical activity of *P. aeruginosa* and electron transfer between an electrode has been reported [23,24]. However, mineral–microorganism interactions may be more complex than we previously thought, especially upon sunlight exposure. To the best of our knowledge, no study of the EET process between semiconducting minerals and *P. aeruginosa* has been reported until now. In this study, we sought to investigate the EET process between mineral photocatalysis of hematite photoanode and *P. aeruginosa*. We believe that our results enhance the understanding of the EET process for microorganism–mineral interactions under light conditions in natural environments.

2. Materials and Methods

2.1. Preparation of the Hematite Electrodes

The hematite electrodes were prepared by anodic electrodeposition coupling with an annealing method, which was performed in a three-electrode electrochemical cell [25]. Fluorine-doped tin oxide (FTO) was used as the working electrode while platinum sheet (1 cm × 1 cm) and an Ag/AgCl electrode in 4 M KCl solution were used as the counter and reference electrode, respectively. FTO should be cleaned in acetone, ethanol, and distilled water by sonication for 30 min in each solvent. Electrodeposition was carried out in an aqueous solution of 0.02 mM FeCl₂. The pH of the freshly prepared plating solution was 4.1. Analytical-grade reagents and 18.3 MΩ Millipore water were used for solutions preparation. The exposed area of the working electrode was 2.5 × 4 cm². Deposition was carried out at 75 °C and a constant potential of 1.2 V (vs. Ag/AgCl) was maintained by an electrochemical workstation (CHI 760E Shanghai Chenhua Instrument, Shanghai, China). The deposition process was controlled with a charge of 1.5 C and then rinsed with distilled water. Finally, the electrodes were annealed in an atmosphere at 520 °C for 120 min and the hematite electrode obtained.

2.2. Bacteria and Growth Conditions

Wild-type *P. aeruginosa* PAO1 was used in this study. The stock solutions of *P. aeruginosa* PAO1 at $-20\text{ }^{\circ}\text{C}$ were aerobically inoculated in 20 mL Luria-Bertani no sodium chloride (LBNS) overnight which had been grown at $37\text{ }^{\circ}\text{C}$. Then, the cell suspension was inoculated in 2% (*v/v*) LBNS for 36 h. Finally, inoculated to 50% (*v/v*) and kept in fed-batch cultivation in a reaction system with a potential of 0.2 V. All of the experiments were carried out at a constant temperature in a humidity incubator ($35 \pm 1\text{ }^{\circ}\text{C}$).

2.3. Characterization of the Hematite Electrodes

The micro-morphologies of the hematite electrode were observed by an Environmental Scanning Electron Microscope (ESEM) (Quanta EFG 450, FEI Company, Hillsboro, OR, USA). Before observation, the electrode was pasted on an aluminum SEM stub by conductive tapes, then gold was sprayed on the surface using a Denton Desk II Gold Sputter Coater. The ESEM was operated at an accelerating voltage of 20 kV and a work distance of 10.6 mm.

Mineral phase analysis of hematite was measured by Raman spectra (Renishaw inVia Reflex, Renishaw Engineering, Wotton-under-Edge, UK) equipped with a 532 nm laser with laser intensity of 50%. A $50\times$ objective with a long working-distance was used and the diameter of the beam spot was $1\text{ }\mu\text{m}$ approximately. The spectra were calibrated with the peak at 520.5 cm^{-1} of a silicon wafer.

The optical band gap of the semiconducting hematite electrode was determined by UV-Vis absorption spectroscopy (UV 3600-Plus, Shimadzu Corp., Kyoto, Japan) with transmission mode. All the spectra were subtracted with the baseline of a bare FTO substrate.

Photoresponse and Mott-Schottky plots of the hematite electrode were measured by a quartz cube cell ($10\text{ cm} \times 10\text{ cm} \times 10\text{ cm}$) with a conventional three-electrode configuration system. The synthetic hematite photoanode was used as the working electrode, a saturated calomel electrode (SCE, 0.244 V vs. normal hydrogen electrode), and a platinum plate ($1\text{ cm} \times 1\text{ cm}$) were used as the working, reference and counter electrode, respectively. Linear sweep voltammetry (LSV) was performed in an electrolyte of $0.1\text{ M Na}_2\text{SO}_4 + 1.0\text{ M}$ methanol from 0 to 1.0 V and with a scan rate of $2\text{ mV}\cdot\text{s}^{-1}$. Dark and light conditions were realized by chopped irradiation from an external simulated LED (Light Emitting Diode) with illumination intensity of $40\text{ mW}\cdot\text{cm}^{-2}$. Mott-Schottky plots were measured at various frequencies of 0.8, 1.0, 1.5 kHz in the same solution as LSV measurement. All the potentials were referred to the SCE electrode unless otherwise stated in this paper.

2.4. Reaction System Configuration and Photoelectrochemical Measurements

The light-hematite-PAO1 system was based on a conventional single-chambered microbial fuel cell (with a liquid volume of 60 mL). A three-electrode configuration, including hematite photoanode, a saturated calomel electrode and a platinum plate in the reaction system. The interelectrode distance between the working electrode and the counter electrode was 1 cm.

The electron transfer ability between electrode and *P. aeruginosa* PAO1 in reaction system was investigated by using a multi-potentiostat (CHI 1000C, CH Instruments Inc., Shanghai, China) at constant temperature of $35\text{ }^{\circ}\text{C}$. The illumination intensity was 30 mW cm^{-2} . The average of dark and light currents for "Hem + PAO1", "FTO + PAO1" and abiotic control "FTO + PAO1" were compared with each other. Then, the effect of temperature for hematite/bacteria electrochemical interaction was investigated by keeping the system at $4\text{ }^{\circ}\text{C}$ for 20 min and comparing the value of LSV. The potential range was from 0.2 V to 0.8 V and with a scan rate of $2\text{ mV}\cdot\text{s}^{-1}$. In addition, more efforts were made to determine if the electron transferring process takes a direct or an indirect route. The I-t curves of the hematite electrode in the system and the replaced new hematite without bacteria on the surface were compared. Furthermore, electrons transferred from the swimming cell and the oxidation of soluble electron shuttles were explored and the current density in "Hem + LBNS + Cells" and "Hem + LBNS"

studied. The performance of the supernatant of the live cell culture was investigated by cyclic voltammetry. The potential range was from -0.6 V to 0.2 V vs. Ag/AgCl and with a scan rate of 50 $\text{mV}\cdot\text{s}^{-1}$.

3. Results and Discussion

3.1. Structure and Morphology Characterization of the Hematite Electrode

The hematite electrodes were prepared by electrophoretic deposition on the FTO electrodes (shown by ESEM in Figure 1a). Microscopic observation revealed the nearly spherical shape of disorderly accumulated nanoparticles, with some nanospheres linked in succession with the size of particles in the range of 40 – 80 nm. Hematite attributes to the D_{3d}^6 crystal space group with seven expected phonon lines were seen in the Raman spectra, consisting of two A_{1g} phonon modes and five E_g phonon modes [26]. For the Raman spectrum of the synthesized electrode presented in Figure 1b, all notable peaks could be ascribed to hematite, including A_{1g} phonon modes (225 and 498 cm^{-1}), E_g phonon modes (247 , 295 , 413 and 612 cm^{-1}) and a second harmonic vibration (1320 cm^{-1}). After the hematite electrode was used in the light-hematite-PAO1 system, no new peak was detected in the Raman spectrum, therefore during the experimental process no new mineral was formed suggesting great stability of the hematite electrode. Furthermore, the Fe concentration in the medium was determined by a modified Ferrozine method as previously reported [10]. However, no Fe^{2+} was detected indicating the electrode was stable and not dissolving. This indicates a good agreement for the results of the Raman investigation.

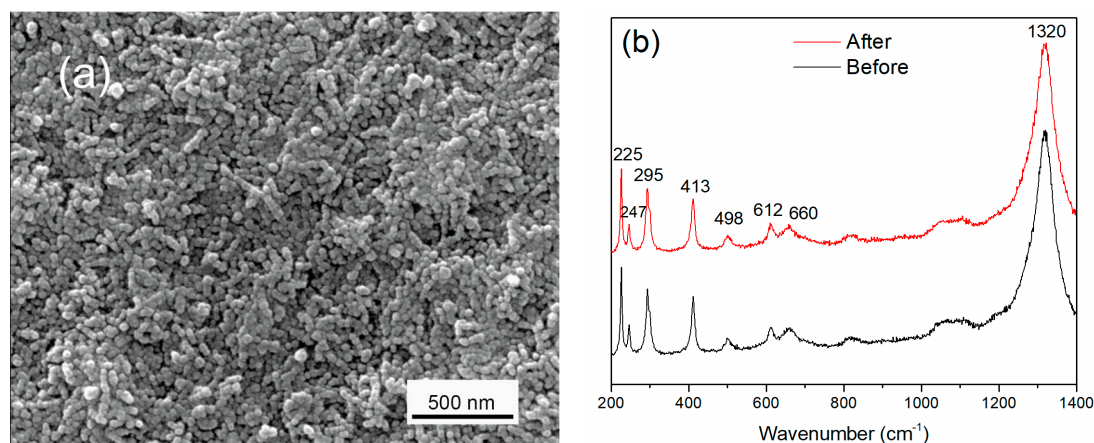


Figure 1. (a) ESEM image of hematite electrode; (b) Raman of hematite electrodes before and after interplay with PAO1.

3.2. Semiconducting Characteristics of Hematite for Band Gap and Flatband Potential

Figure 2 (Insert picture) showed the UV-visible absorption spectrum of the hematite electrode. In the wavelength range of 300 – 700 nm, hematite exhibited a broad absorption. In addition, the maximum absorption wavelength was around 396 nm, and the band gap absorption edge was around 564 nm. The optical absorption of hematite was mainly attributed to indirect transition, although some groups have reported evidence for direct transition [27,28]. The absorption in the UV region is usually caused by a direct charger transition, corresponding to the ligand–metal transfer from $\text{O}^{2-}(2p)$ to $\text{Fe}^{3+}(3d)$. As far as the absorption in the visible light region was concerned, this was attributed to an indirect charger transition, due to metal–metal transfer from 2Fe^{3+} to Fe^{2+} and Fe^{4+} [29]. The Tauc plots and absorption spectrum for hematite are shown in Figure 2. The extrapolated results indicated an allowed indirect band gap of 2.0 eV and an allowed direct band gap of 2.2 eV ($\lambda = 563.6$ nm). This was in accordance with the band gap of hematite, and agrees well with the

previously reported results [30,31]. Based on the laboratory findings with different hematite films, we concluded that the hematite electrode was a visible light photoactive material.

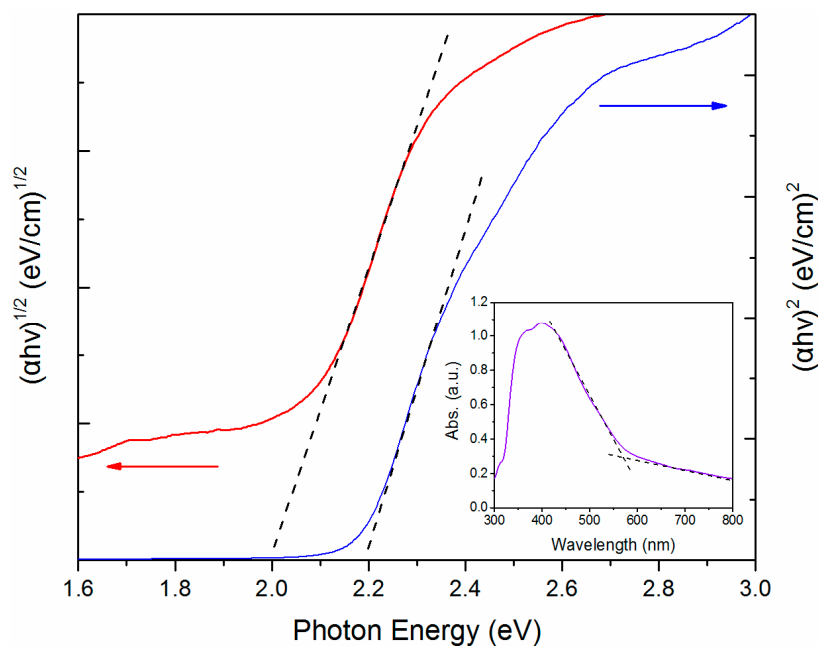


Figure 2. Tauc plots of hematite for determining the indirect (2.0 eV) and direct (2.2 eV) band gaps (Insert picture: UV-Vis absorption spectra for hematite electrode).

The flatband potential is a fundamental property indicating the band structure of the electrode surface at the electrode-solution interface for a semiconductor-electrolyte system, whose values may be determined electrochemically through Mott-Schottky plots [32]. To estimate the flatband position for the hematite electrode, electrochemical impedance studies were carried out with an electrolyte of 0.1 M Na₂SO₄ + 1.0 M methanol. The Mott-Schottky equation relates the capacitance of the semiconductor to the carrier concentration (N_d) and the other constants such as the fundamental charge constant (e), vacuum permittivity (ϵ_0), dielectric constant (ϵ), electrode area (A), and the flatband potential (E_{fb}) as shown in the following Equation (1).

$$\frac{1}{C^2} = \frac{2}{e\epsilon\epsilon_0 A^2 N_d} \left(E - E_{fb} - \frac{kT}{q} \right) \quad (1)$$

Plotting $1/C^2$ versus V allows the estimation of the flatband which could be calculated from the X-intercept. The characteristic Mott-Schottky plots for the hematite electrode measured at various ac frequencies 0.8, 1.0, and 1.5 kHz are shown in Figure 3. The positive slope of these lines indicated that the hematite electrode exhibits photoactivity with n -type behavior. Moreover, the value of the flatbands were all located at -0.08 V vs. SCE for all the three measured ac frequencies, indicating that the flatband of the hematite electrode had a very low dispersion potential which was not frequency dependent [30].

3.3. Photoelectrochemical Characteristics of Hematite

With the aim of evaluating the photo-electrochemical properties of the hematite electrode, electrochemical measurements were carried out. Figure 4 shows the LSV curve of the hematite electrode responding to different potentials in dark and visible light illumination conditions. The dark condition showed a very small current approximately equal to zero. Upon light illumination, the measurable photocurrent increased from $2.07 \mu\text{A}$ at 0.2 V to $13.59 \mu\text{A}$ at 0.8 V vs. SCE and the photocurrent rapidly

went back to the base line when the light was switched off. As a semiconductor, the hematite electrode adsorbed light energy, then photoexcited electrons and holes could be generated. The photocurrent was potential dependent, which increased as the applied potentials were scanned towards a more positive potential indicating that the separation of electron–hole pairs was more effective with higher anodic potential, resulting in the increase of the current output to a certain extent under light illumination [17]. The anodic photocurrents corresponding to the photo-oxidation process indicated that hematite had an *n*-type semiconducting nature which was in accord with the results of the Mott–Schottky plots. Therefore, based on the results above, we concluded that the hematite electrode was a semiconducting mineral which could be activated by visible light. In addition, after the hematite electrode was used in the reaction system with PAO1, there was no obvious change in the current, which indicated the hematite was stable which was consistent with the results of the Raman spectrum.

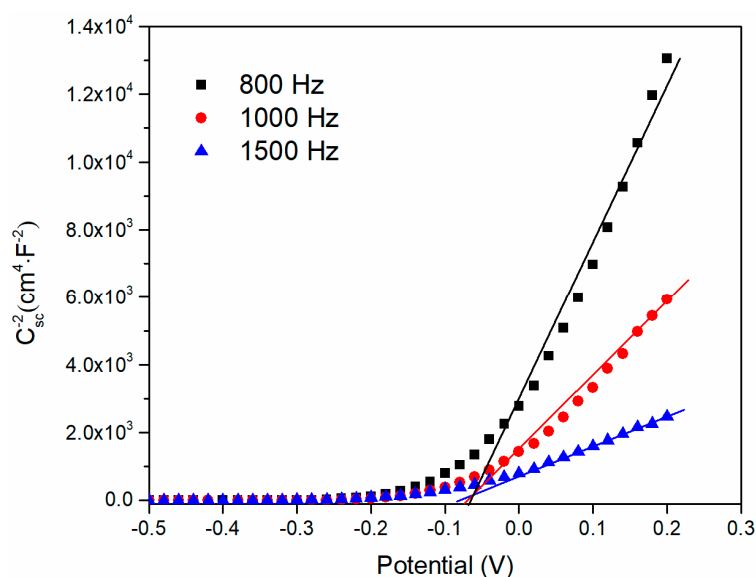


Figure 3. Mott–Schottky plot of the hematite electrode measured at 0.8, 1.0, 1.5 kHz under dark conditions.

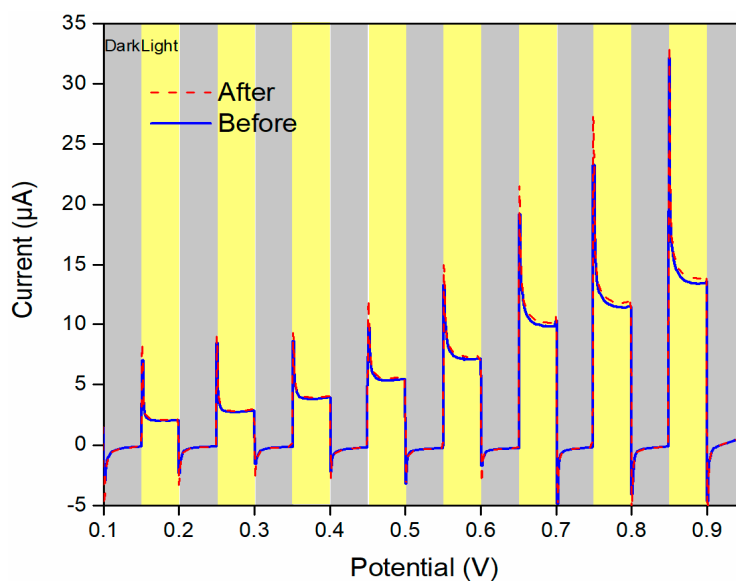


Figure 4. Linear sweep voltammogram of the hematite electrode in dark/light conditions showing *n*-type photocurrent and reasonable catalytic activity.

3.4. Enhanced Electron Transfer Capability in the Light-Hematite-PAO1 System

The performance of the hematite photoelectrode in the light-hematite-PAO1 system with or without wild-type PAO1 was studied. The results of the amperometric I-t curves measurements (Figure 5) showed that, the system produced negligible current without PAO1 in dark conditions. When PAO1 was present, the average current generated was $3.0 \pm 0.1 \mu\text{A}/\text{cm}^2$ and $4.1 \pm 0.1 \mu\text{A}/\text{cm}^2$ at the FTO and hematite electrode surface. The higher value of current in “Hem+PAO1” might be due to the specific surface area of the hematite being much larger than the FTO electrode. In the dark, electron transport was thought to occur in the conduction band Fe(3d) through the hematite electrode, while at this time the charges in the valence band O(2p) were not free-flowing unless excited by light or heat [33].

With light illumination, the abiotic control generated a measurable average photocurrent of $7.5 \pm 0.2 \mu\text{A}/\text{cm}^2$ in the LBNS electrolyte. In previous studies, a similar incensement of photocurrent density was observed in abiotic control experiments with light illumination, which was attributed to the photocatalytic reactions of the photoelectrode [17,18]. The average photocurrent output for the light-hematite-PAO1 system reached $18.1 \pm 0.2 \mu\text{A}/\text{cm}^2$ under light illumination, which was almost 2.4 times higher than that of the value of the abiotic control under the same conditions. Moreover, it is worthwhile mentioning that this was only $0.6 \mu\text{A}/\text{cm}^2$ higher than the dark current in the “FTO + PAO1” experimental group, which suggests that the light had a negligible effect on PAO1. Therefore, the significant enhanced current output in “Hem + PAO1” could be ascribed to the transfer of bioelectrons from PAO1 to the hematite anode and subsequently the external circuit. When the hematite electrode was irradiated by visible light, photoexcited holes prepared at the valence band of the hematite could combine with bioelectrons and more electrons flowed into the external circuit.

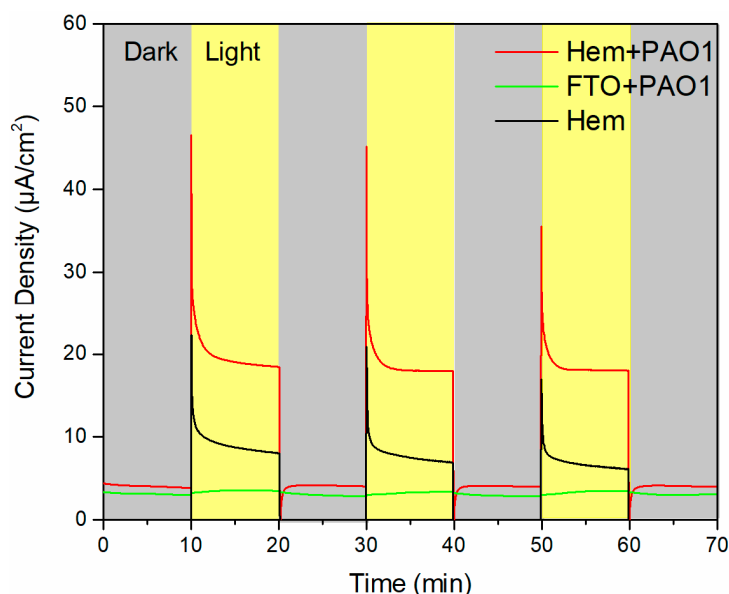


Figure 5. Amperometric I-t curves of the light-hematite-PAO1 system with different conditions under light on/off cycles.

3.5. Bioelectrochemistry Activity in the System Influenced by Temperature

To further confirm that the enhanced current was due to bioelectrochemical processes for transferring bioelectrons from PAO1 to hematite anode, the effect of temperature on the hematite/bacteria electrochemical interaction was investigated. After completing the room temperature test, the light-hematite-PAO1 system was kept at $4 \text{ }^\circ\text{C}$ for 20 min and used for further investigation. LSV in the potential range of 0.2 V to 0.8 V was carried out and the results are shown in Figure 6. At room temperature, the average dark current was $6.8 \mu\text{A}$ and the light current increased

from 23.7 μA at 0.3 V to 44.7 μA at 0.8 V. In comparison, when the system was cold treated, the dark current decreased to 1.4 μA which was only one fifth of the previous value. Moreover, the light current decreased more significantly, whose values were only 15.1 μA at 0.3 V and 24.5 μA at 0.8 V, respectively. In addition, the light current was little changed, although with higher applied potentials, which may be limited by the rate of the biocatalytic reactions. After the system returned to room temperature the current increased. These results indicated that the number of electrons was influenced by the activity of the cells and implied the bioelectrochemical process was considerable. It is rational that the photoanode hematite was able to harvest bioelectrons from the microorganisms in addition to solar energy. Therefore, the behavior of the positive relationship between the system current and temperature led us to conclude that bioelectrochemical processes of PAO1 played a significant role in enhancing electron transfer under light.

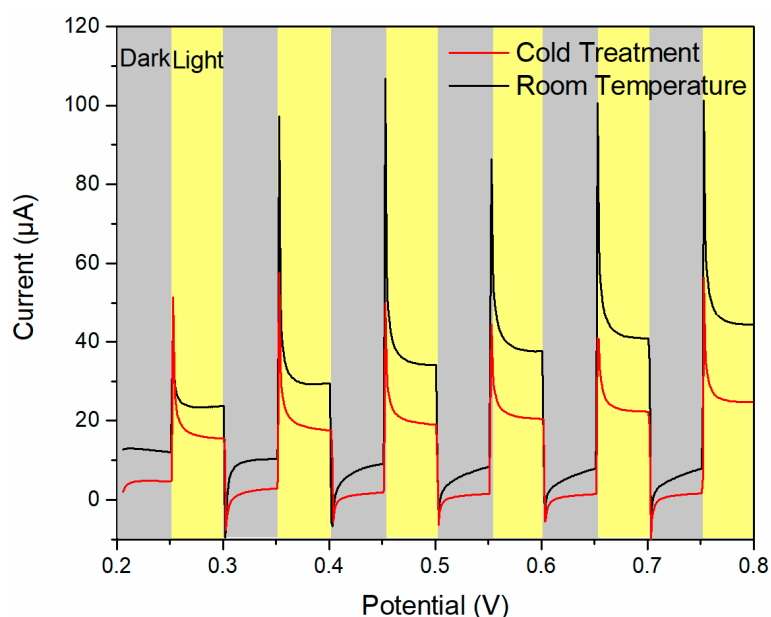


Figure 6. Amperometric I-t curves of the the light-hematite-PAO1 system with different conditions under light on/off cycles.

3.6. Direct/Indirect Electron Transfer between the Hematite and PAO1

Previous study showed that direct electron transfer from *G. sulfurreducens* cells to hematite could occur in the absence of soluble electron shuttles under light [16]. In order to thoroughly investigate the electron transfer process between hematite and PAO1 belonging to a direct or an indirect route, the electrode in system was replaced by a new hematite which had no bacteria on the surface. As shown in Figure 7 (marked as line “New Hem + PAO1”), the value of the current density was nearly invariable in dark conditions. However, the value of the average photocurrent decreased 1.8 $\mu\text{A}/\text{cm}^2$ approximately, which could be attributed to the contribution of direct electron transfer by PAO1 and may be realized by extracellular conductive components (such as pili). Subsequently, the bio-photoanode was observed by light microscopy (Leica DMI8, Leica Microsystems, Wetzlar, Germany), and some bacterial cells were distributed on the hematite surface. The ESEM image of the electrode showed that these cells had a rod-shaped morphology and dispersed randomly (Figure S1, Supplementary Materials). Therefore, some cells stayed on the hematite surface and direct electron transfers occurred in the light-hematite-PAO1 system, however this only accounted for a small proportion.

In order to demonstrate that the indirect electron transfer route played a significant role in the system, the live cell culture was taken out and new LBNS injected into the device. The I-t curves with the new LBNS medium were examined (marker as “Hem + LBNS”). As shown in Figure 7,

the photocurrent density decreased from $19.5 \pm 0.5 \mu\text{A}/\text{cm}^2$ to $7.6 \pm 0.3 \mu\text{A}/\text{cm}^2$, which comes to a similar level as the abiotic control in Section 3.4. Taking the above results into account, we could conclude that the indirect transfer route of live cell culture may have played a critical role in enhancing electron transfer. Furthermore, the live cell culture was centrifuged at 10,000 r/min for 5 min, then after removing the supernatant and resuspending the cell pellet into the device containing the new LBNS and new hematite electrode, the current density in “Hem + LBNS + Cells” was only $7.9 \pm 0.2 \mu\text{A}/\text{cm}^2$ with a negligible current growth of less than $0.3 \mu\text{A}/\text{cm}^2$ compared with the “Hem + LBNS”. The results indicated that only a few electrons were probably donated by the swimming cells. Hence, more effort should be made to explore the soluble matters concerning the electron transfer process.

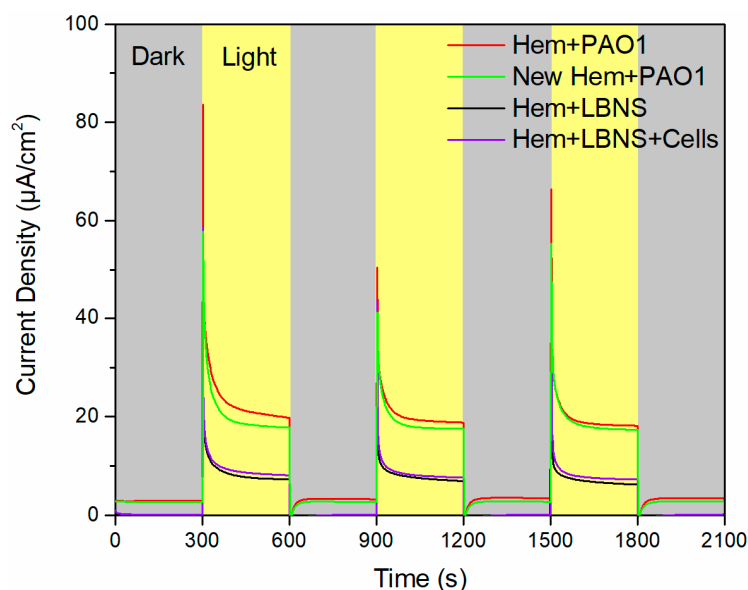


Figure 7. Amperometric I-t curves of the light-hematite-PAO1 system with different conditions under light on/off cycles.

As reported previously, *P. aeruginosa* could produce phenazines (such as pyocyanin, 1-hydroxyphenazine, phenazine-1-carboxylate, etc.) as soluble redox mediators to enhance electron transport [23,34,35]. Cyclic voltammetry (CV) was used to investigate the performance of supernatant from live cell culture. The results showed that a pair of redox peaks were identified and the positions of the oxidation and reduction peaks were -200 mV and -280 mV vs. Ag/AgCl respectively (Figure S2, Supplementary Materials), suggesting active electron transfer could occur in the supernatant. Moreover, different phenazine compounds had different redox potentials, the CV results were consistent with the value of pyocyanin [35]. On the basis of these results, redox-active pyocyanin may play a significant role for indirect electron transfer between hematite and PAO1 under light. To further confirm that the main soluble redox mediators were pyocyanins, we isolated them successfully in supernatant from centrifuged live cell culture as described elsewhere [36] (Figure S3, Supplementary Materials). To gain more insight, we further confirmed them by surface-enhanced Raman scattering (SERS) measurement. The results well-matched the Raman signals of pyocyanin (Figure S4, Supplementary Materials). Accordingly, we concluded that what really is of consequence in the process of enhanced electron transfer between hematite and PAO1 occurred by the indirect route and probably mainly relies on the soluble pyocyanin biosynthesized by *P. aeruginosa* PAO1.

3.7. Mechanistic for Enhanced Electron Transfer between Hematite and PAO1 under Light

As mentioned above, the research on interactions of light-semiconducting mineral-microorganism systems is still in its infancy. On the one hand, we have the complexity of the system involving both

bioelectrogenesis and photocatalysis. Previous studies have shown that under light irradiation TiO_2 could destroy the cellular structure of microorganisms [37]. However, there is no denying that the band gap and positions of the energy bands determined the properties of the semiconductor. As a more moderate semiconductor, it is interesting that hematite preformed a harmonious relationship with different microorganisms. On the other hand, there was thereby an urgent need which was still a significant challenge to study many more bacteria in addition to *Geobacter* and *Shewanella*.

Based on the results in this study, the proposed schematic mechanism of visible light enhanced extracellular electron transfer between hematite and PAO1 is shown in Figure 8. During the process of metabolism, bioelectrons were produced and transferred to the extracellular conductive components. Moreover, soluble electron shuttles were biosynthesized and diffused in solution. In dark conditions, bioelectrons were injected into the $\text{Fe}(3d)$ conduction band on the hematite surface and were delivered to the FTO substrate. Under light illumination, the semiconducting property of hematite was activated leading to a better conductivity generating holes in the $\text{O}(2p)$ valence band. At the same time, the photoexcited holes in the valence band $\text{O}(2p)$ became free-flowing, which could more easily combine with the bioelectrons because of a more positive potential. Then, a more efficient electron transfer process occurred on the surface of the hematite which resulted in a higher current output. Most of the bioelectrons come from pyocyanin and a small proportion of them from the direct transfer route. When the hematite electrode was excited by light, the bioelectrons reacted with the photoexcited holes. With the help of holes on the hematite surface, hematite no longer acted as the electron acceptor. Finally, the bioelectron delivered to the external circuit and was protected rather than dissolving which was confirmed by the results of the Raman, Fe concentration test and LSV of the hematite electrodes.

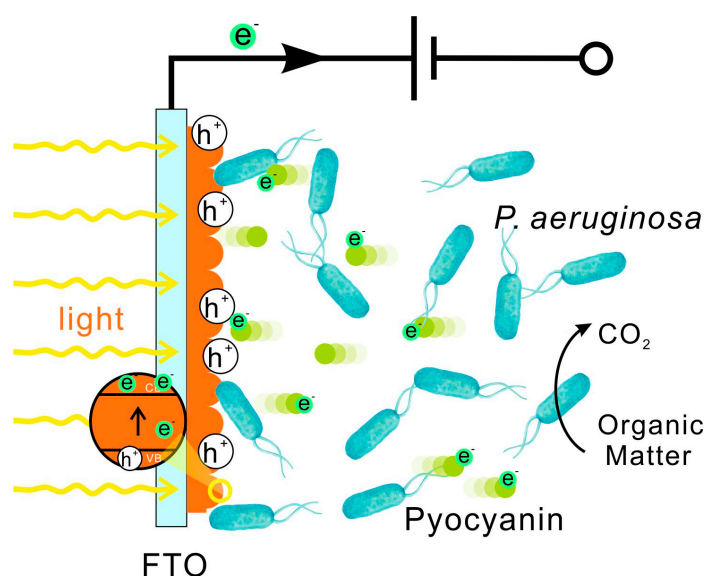


Figure 8. Schematic diagram of the electron transferring process between hematite and PAO1 under visible light irradiation.

Iron and manganese are common variable valence elements in nature. Due to their distinct redox chemistry with low solubility of the oxidized species from oxyhydroxides, iron and manganese oxide are widely distributed on the surface of the earth's environmental system, such as in desert varnish, soil particles, and ferromanganese crust of weathering [38–40]. However, their semiconducting properties have been neglected for a long time. The number of prokaryotes on earth has been estimated to be $4\text{--}6 \times 10^{30}$ cells and they are found nearly everywhere [41]. The interactions between minerals and bacteria under sunlight irradiation have been going on for quite a long geological history. The results of the present study might be helpful to understand the processes of electron transfer related to the interactions between semiconducting minerals and bacteria under sunlight irradiation

in earth surface environments. In addition, the investigation of electron transfers between minerals photocatalysis, and microorganisms under solar illumination will probably be useful for solar energy utilization and electricity generation in the future.

4. Conclusions

In this study, we investigated for the first time the enhanced electrochemical interaction between hematite photoanode and *P. aeruginosa* PAO1. Hematite electrode was prepared by anodic electrodeposition, which was characterized by ESEM and Raman spectroscopy. Moreover, UV–Vis spectroscopy was used to determine the value of the band gap and electrochemical techniques indicated that hematite was a photoactive material responsive to visible light. Under light illumination, a photocurrent density output for light-hematite-PAO1 system reached $18.1 \pm 0.2 \mu\text{A}/\text{cm}^2$, which was almost 2.4 times higher than that in abiotic control. Different temperatures of LSV measurement of the system indicated the enhanced current was due to bioelectrochemical processes. Furthermore, amperometric I–t curves in different mediums showed that both direct and indirect electron transferring process occurred between the hematite photoanode and PAO1. In addition, the indirect route was primary and probably mainly relies on pyocyanin biosynthesized by PAO1. Therefore, in addition to *Geobacter* and *Shewanella*, more bacteria are able to perform the enhanced extracellular electron transfer process with semiconducting minerals under light. Our results have expanded our understanding of the EET of microorganisms and the photocatalysis of semiconducting minerals in natural environments.

Supplementary Materials: The following are available online at www.mdpi.com/2075-163X/7/12/230/s1, Figure S1: (a) Light microscopy picture of bio-photoanode; (b) ESEM picture of bio-photoanode, Figure S2: Cyclic voltammetry results of the supernatant from live cell culture and fresh LBNS, Figure S3: (a) Pyocyanin in live cell culture; (b) Liquid-liquid extraction for pyocyanin by CHCl_3 ; (c) Liquid-liquid extraction for pyocyanin by HCl, Figure S4: SERS spectra of pyocyanin isolated from centrifuged supernatant of live cell culture.

Acknowledgments: This work was funded by the National Basic Research Program of China (973 Program) (Grant No. 2014CB846001) and the Natural Science Foundation of China (Grant No. 41230103, 41522201 & 41402032). We thank Yifeng Jiang for her technical assistance in SEM sample preparation and image analysis at the Core Facilities of College of Life Science, Peking University.

Author Contributions: Guiping Ren and Hongrui Ding conceived and designed the experiments; Guiping Ren, Yuan Sun and Manyi Sun performed the experiments; Guiping Ren analyzed the data; Guiping Ren wrote the paper; Hongrui Ding, Anhuai Lu, and Yan Li performed revisions; Hongrui Ding and Anhuai Lu gave final approval of the version to be published; Anhuai Lu funded the study.

Conflicts of Interest: The authors declare no conflict of interest.

References

1. Myers, C.R.; Neelson, K.H. Bacterial manganese reduction and growth with manganese oxide as the sole electron acceptor. *Science* **1988**, *240*, 1319–1321. [[CrossRef](#)] [[PubMed](#)]
2. Summers, Z.M.; Fogarty, H.E.; Leang, C.; Franks, A.E.; Malvankar, N.S.; Lovley, D.R. Direct exchange of electrons within aggregates of an evolved syntrophic coculture of anaerobic bacteria. *Science* **2010**, *330*, 1413–1415. [[CrossRef](#)] [[PubMed](#)]
3. Kato, S.; Hashimoto, K.; Watanabe, K. Microbial interspecies electron transfer via electric currents through conductive minerals. *Proc. Natl. Acad. Sci. USA* **2012**, *109*, 10042–10046. [[CrossRef](#)] [[PubMed](#)]
4. Liu, X.W.; Li, W.W.; Yu, H.Q. Cathodic catalysts in bioelectrochemical systems for energy recovery from wastewater. *Chem. Soc. Rev.* **2014**, *43*, 7718–7745. [[CrossRef](#)] [[PubMed](#)]
5. Lovley, D.R. Live wires: Direct extracellular electron exchange for bioenergy and the bioremediation of energy-related contamination. *Energy Environ. Sci.* **2011**, *4*, 4896–4906. [[CrossRef](#)]
6. Lovley, D.R.; Nevin, K.P. A shift in the current: New applications and concepts for microbe–electrode electron exchange. *Curr. Opin. Biotechnol.* **2011**, *22*, 441–448. [[CrossRef](#)] [[PubMed](#)]
7. Shi, L.; Dong, H.; Reguera, G.; Beyenal, H.; Lu, A.; Liu, J.; Yu, H.Q.; Fredrickson, J.K. Extracellular electron transfer mechanisms between microorganisms and minerals. *Nat. Rev. Microbiol.* **2016**, *14*, 651–662. [[CrossRef](#)] [[PubMed](#)]
8. Lovley, D.R. Dissimilatory Fe (III) and Mn (IV) reduction. *Microbiol. Rev.* **1991**, *55*, 259–287. [[PubMed](#)]

9. Weber, K.A.; Achenbach, L.A.; Coates, J.D. Microorganisms pumping iron: Anaerobic microbial iron oxidation and reduction. *Nat. Rev. Microbiol.* **2006**, *4*, 752–764. [[CrossRef](#)] [[PubMed](#)]
10. Ren, G.; Ding, H.; Li, Y.; Lu, A. Natural Hematite as a Low-Cost and Earth-Abundant Cathode Material for Performance Improvement of Microbial Fuel Cells. *Catalysts* **2016**, *6*, 157. [[CrossRef](#)]
11. Nakamura, R.; Kai, F.; Okamoto, A.; Newton, G.J.; Hashimoto, K. Self-constructed electrically conductive bacterial networks. *Angew. Chem. Int. Edit.* **2009**, *48*, 508–511. [[CrossRef](#)] [[PubMed](#)]
12. Xu, Y.; Schoonen, M.A. The absolute energy positions of conduction and valence bands of selected semiconducting minerals. *Am. Mineral.* **2000**, *85*, 543–556. [[CrossRef](#)]
13. Lu, A.; Li, Y.; Jin, S.; Wang, X.; Wu, X.; Zeng, C.; Li, Y.; Ding, H.; Hao, R.; Lv, M.; et al. Growth of non-phototrophic microorganisms using solar energy through mineral photocatalysis. *Nat. Commun.* **2012**, *3*, 768. [[CrossRef](#)] [[PubMed](#)]
14. Sakimoto, K.K.; Wong, A.B.; Yang, P. Self-photosensitization of nonphotosynthetic bacteria for solar-to-chemical production. *Science* **2016**, *351*, 74–77. [[CrossRef](#)] [[PubMed](#)]
15. Kornienko, N.; Sakimoto, K.K.; Herlihy, D.M.; Nguyen, S.C.; Alivisatos, A.P.; Harris, C.B.; Schwartzberg, A.; Yang, P. Spectroscopic elucidation of energy transfer in hybrid inorganic–biological organisms for solar-to-chemical production. *Proc. Natl. Acad. Sci. USA* **2016**, *113*, 11750–11755. [[CrossRef](#)] [[PubMed](#)]
16. Li, D.B.; Cheng, Y.Y.; Li, L.L.; Li, W.W.; Huang, Y.X.; Pei, D.N.; Tong, Z.H.; Mu, Y.; Yu, H.Q. Light-driven microbial dissimilatory electron transfer to hematite. *Phys. Chem. Chem. Phys.* **2014**, *16*, 23003–23011. [[CrossRef](#)] [[PubMed](#)]
17. Qian, F.; Wang, H.; Ling, Y.; Wang, G.; Thelen, M.P.; Li, Y. Photoenhanced electrochemical interaction between *Shewanella* and a hematite nanowire photoanode. *Nano Lett.* **2014**, *14*, 3688–3693. [[CrossRef](#)] [[PubMed](#)]
18. Zhu, G.; Yang, Y.; Liu, J.; Liu, F.; Lu, A.; He, W. Enhanced photocurrent production by the synergy of hematite nanowire-arrayed photoanode and bioengineered *Shewanella oneidensis* MR-1. *Biosens. Bioelectron.* **2017**, *94*, 227–234. [[CrossRef](#)] [[PubMed](#)]
19. Feng, H.; Liang, Y.; Guo, K.; Li, N.; Shen, D.; Cong, Y.; Zhou, Y.; Wang, Y.; Wang, M.; Long, Y. Hybridization of photoanode and bioanode to enhance the current production of bioelectrochemical systems. *Water Res.* **2016**, *102*, 428–435. [[CrossRef](#)] [[PubMed](#)]
20. Klockgether, J.; Munder, A.; Neugebauer, J.; Davenport, C.F.; Stanke, F.; Larbig, K.D.; Heeb, S.; Schöck, U.; Pohl, T.M.; Wiehlmann, L.; et al. Genome diversity of *Pseudomonas aeruginosa* PAO1 laboratory strains. *J. Bacteriol.* **2010**, *192*, 1113–1121. [[CrossRef](#)] [[PubMed](#)]
21. Rabaey, K.; Boon, N.; Siciliano, S.D.; Verhaege, M.; Verstraete, W. Biofuel cells select for microbial consortia that self-mediate electron transfer. *Appl. Environ. Microbiol.* **2004**, *70*, 5373–5382. [[CrossRef](#)] [[PubMed](#)]
22. Rahme, L.G.; Ausubel, F.M.; Cao, H.; Drenkard, E.; Goumnerov, B.C.; Lau, G.W.; Mahajan-Miklos, S.; Plotnikova, J.; Tan, M.W.; Tsongalis, J.; et al. Plants and animals share functionally common bacterial virulence factors. *Proc. Natl. Acad. Sci. USA* **2000**, *97*, 8815–8821. [[CrossRef](#)] [[PubMed](#)]
23. Rabaey, K.; Boon, N.; Höfte, M.; Verstraete, W. Microbial phenazine production enhances electron transfer in biofuel cells. *Environ. Sci. Technol.* **2005**, *39*, 3401–3408. [[CrossRef](#)] [[PubMed](#)]
24. Hernandez, M.E.; Kappler, A.; Newman, D.K. Phenazines and other redox-active antibiotics promote microbial mineral reduction. *Appl. Environ. Microbiol.* **2004**, *70*, 921–928. [[CrossRef](#)] [[PubMed](#)]
25. Spray, R.L.; Choi, K.S. Photoactivity of transparent nanocrystalline Fe₂O₃ electrodes prepared via anodic electrodeposition. *Chem. Mater.* **2009**, *21*, 3701–3709. [[CrossRef](#)]
26. De Faria, D.L.A.; Venâncio Silva, S.; De Oliveira, M.T. Raman microspectroscopy of some iron oxides and oxyhydroxides. *J. Raman Spectrosc.* **1997**, *28*, 873–878. [[CrossRef](#)]
27. Duret, A.; Grätzel, M. Visible light-induced water oxidation on mesoscopic α -Fe₂O₃ films made by ultrasonic spray pyrolysis. *J. Phys. Chem. B* **2005**, *109*, 17184–17191. [[CrossRef](#)] [[PubMed](#)]
28. Zhang, Z.; Hossain, M.F.; Takahashi, T. Self-assembled hematite (α -Fe₂O₃) nanotube arrays for photoelectrocatalytic degradation of azo dye under simulated solar light irradiation. *Appl. Catal. B* **2010**, *95*, 423–429. [[CrossRef](#)]
29. Kay, A.; Cesar, I.; Grätzel, M. New benchmark for water photooxidation by nanostructured α -Fe₂O₃ films. *J. Am. Chem. Soc.* **2006**, *128*, 15714–15721. [[CrossRef](#)] [[PubMed](#)]
30. Khan, S.U.M.; Akikusa, J. Photoelectrochemical splitting of water at nanocrystalline n-Fe₂O₃ thin-film electrodes. *J. Phys. Chem. B* **1999**, *103*, 7184–7189. [[CrossRef](#)]

31. Miller, E.L.; Paluselli, D.; Marsen, B.; Rocheleau, R.E. Low-temperature reactively sputtered iron oxide for thin film devices. *Thin Solid Films* **2004**, *466*, 307–313. [[CrossRef](#)]
32. Gelderman, K.; Lee, L.; Donne, S.W. Flat-band potential of a semiconductor: Using the Mott–Schottky equation. *J. Chem. Educ.* **2007**, *84*, 685. [[CrossRef](#)]
33. Sherman, D.M. Electronic structures of iron (III) and manganese (IV) (hydr) oxide minerals: Thermodynamics of photochemical reductive dissolution in aquatic environments. *Geochim. Cosmochim. Acta* **2005**, *69*, 3249–3255. [[CrossRef](#)]
34. Pham, T.H.; Boon, N.; De Maeyer, K.; Hofte, M.; Rabaey, K.; Verstraete, W. Use of Pseudomonas species producing phenazine-based metabolites in the anodes of microbial fuel cells to improve electricity generation. *Appl. Microbiol. Biotechnol.* **2008**, *80*, 985–993. [[CrossRef](#)] [[PubMed](#)]
35. Wang, Y.; Newman, D.K. Redox reactions of phenazine antibiotics with ferric (hydr) oxides and molecular oxygen. *Environ. Sci. Technol.* **2008**, *42*, 2380–2386. [[CrossRef](#)] [[PubMed](#)]
36. Essar, D.W.; Eberly, L.; Hadero, A.; Crawford, I.P. Identification and characterization of genes for a second anthranilate synthase in Pseudomonas aeruginosa: Interchangeability of the two anthranilate synthases and evolutionary implications. *J. Bacteriol.* **1990**, *172*, 884–900. [[CrossRef](#)] [[PubMed](#)]
37. Maness, P.C.; Smolinski, S.; Blake, D.M.; Huang, Z.; Wolfrum, E.J.; Jacoby, W.A. Bactericidal activity of photocatalytic TiO₂ reaction: Toward an understanding of its killing mechanism. *Appl. Environ. Microbiol.* **1999**, *65*, 4094–4098. [[PubMed](#)]
38. Koschinsky, A.; Halbach, P. Sequential leaching of marine ferromanganese precipitates: Genetic implications. *Geochim. Cosmochim. Acta* **1995**, *59*, 5113–5132. [[CrossRef](#)]
39. Manheim, F.T.; Lane-Bostwick, C.M. Cobalt in ferromanganese crusts as a monitor of hydrothermal discharge on the Pacific sea floor. *Nature* **1988**, *335*, 59–62. [[CrossRef](#)]
40. Boston, P.J.; Spilde, M.N.; Northup, D.E.; Dichosa, A. Biogenic Fe/Mn oxides in caves and surface desert varnish: Potential biosignatures for Earth and Mars. *Astrobiology* **2008**, *8*, 448.
41. Whitman, W.B.; Coleman, D.C.; Wiebe, W.J. Prokaryotes: The unseen majority. *Proc. Natl. Acad. Sci. USA* **1998**, *95*, 6578–6583. [[CrossRef](#)] [[PubMed](#)]



© 2017 by the authors. Licensee MDPI, Basel, Switzerland. This article is an open access article distributed under the terms and conditions of the Creative Commons Attribution (CC BY) license (<http://creativecommons.org/licenses/by/4.0/>).